Inorganic Chemistry

Article

pubs.acs.org/IC

Gas-Phase Uranyl, Neptunyl, and Plutonyl: Hydration and Oxidation Studied by Experiment and Theory

Daniel Rios,[†] Maria C. Michelini,*[,‡] Ana F. Lucena,[§] Joaquim Marçalo,[§] Travis H. Bray,[†] and John K. Gibson*[,†]

[†]Chemical Sciences Division, Lawrence Berkeley National Laboratory, Berkeley, California 94720, United States

[‡]Dipartimento di Chimica, Università della Calabria, 87030 Arcavacata di Rende, Italy

[§]Unidade de Ciências Químicas e Radiofarmacêuticas, Instituto Tecnológico e Nuclear, Instituto Superior Técnico, 2686-953 Sacavém, Portugal

Supporting Information

ABSTRACT: The following monopositive actinyl ions were produced by electrospray ionization of aqueous solutions of $An^{VI}O_2(ClO_4)_2$ (An = U, Np, Pu): $U^{V}O_2^{+}$, $Np^{V}O_2^{+}$, $Pu^{V}O_2^{+}$, $U^{VI}O_2(OH)^{+}$, and $Pu^{VI}O_2(OH)^{+}$; abundances of the actinyl ions reflect the relative stabilities of the An(VI) and An(V) oxidation states. Gas-phase reactions with water in an ion trap revealed that water addition terminates at $AnO_2^{+}\cdot(H_2O)_4$ (An = U, Np, Pu) and $AnO_2(OH)^{+}\cdot(H_2O)_3$ (An = U, Pu), each with four equatorial ligands. These terminal hydrates evidently correspond to the maximum inner-sphere water coordination in the gas phase, as substantiated by density functional theory (DFT) computations of the hydrate structures and energetics. Measured hydration rates for the $AnO_2(OH)^{+}$ were substantially faster than for the AnO_2^{+}, reflecting additional vibrational degrees of freedom in the hydroxide ions for stabilization of hot adducts. Dioxygen addition resulted in $UO_2^{+}(O_2)(H_2O)_n$ (n = 2, 3), whereas O_2 addition was not observed for NpO_2^{+} or PuO_2^{+} hydrates. DFT suggests that two-electron three-centered bonds form between UO_2^{+} and O_2, but not between NpO_2^{+} and O_2. As formation of the $UO_2^{+}-O_2$ bonds formally corresponds to the oxidation of U(V) to U(VI), the absence of this bonding with NpO_2^{+} can be considered a manifestation of the lower relative stability of Np(VI).

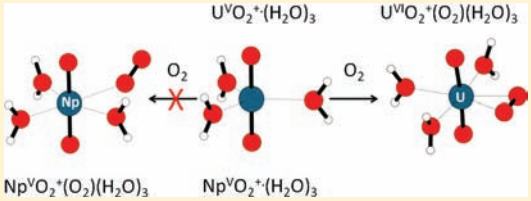

INTRODUCTION

The preponderance of actinide chemistry occurs in the presence of water, commonly in aqueous solutions. The distinctive linear monopositive and dipositive actinyl ions, $\{O{=}An{=}O\}^{+,2+}$, are particularly important species in much of the solution chemistry of uranium, neptunium, and plutonium.[1,2] The addition of water to actinyl ions in the gas phase, as described here, presents the most elementary basis to understanding the fundamental phenomenon of hydration absent perturbations introduced in condensed phases. Among the key properties in the gas phase which can be experimentally determined are kinetics for water addition and the terminal extent of inner-sphere hydration. Previous experimental studies of gas-phase hydration of UO_2^{+} and $UO_2(OH)^{+}$ have determined the kinetics of water addition, and the maximum number of added water ligands.[3,4] In that work, it was found that UO_2^{+} and $UO_2(OH)^{+}$ add up to four and three water molecules, respectively, resulting in a uranyl coordination number of four. Although aqueous $U^{V}O_2^{+}$ is generally unstable toward disproportionation into U^{IV} and $U^{VI}O_2^{2+}$, according to eq 1[5] there is evidence that the solution hydration characteristics of UO_2^{+}, NpO_2^{+}, and PuO_2^{+} are generally similar, with an (average) inner-sphere hydration number of five.[6]

$$2UO_2^{+} + 4H^{+} \rightarrow U^{4+} + UO_2^{2+} + 2H_2O \quad (1)$$

The inner-sphere hydration number of the aqueous dipositive AnO_2^{2+} ions (An = U, Np, Pu) has also been determined to be approximately five,[6,7] with the caveat that in solution inner-sphere coordination is not static, and there is likely a dynamic equilibrium between four and five inner-sphere waters.[8] Considering the recent computational results of Bühl et al.,[9] it can be surmised that water coordination of cationic metal centers is enhanced in solution by electron donation from second-shell water molecules, which effectively renders the inner sphere water molecules as better Lewis bases. A result is that inner-sphere hydration in the gas-phase should generally be less than that in solution, evidently by one water ligand in the case of UO_2^{+}. Despite the fact that hydration in the gas phase predictably does not directly reveal that in solution, it can provide important insights, including variations across the actinide series as well as differences due to changes in ligation and oxidation state.

As a crucial complement to gas-phase experimental studies in which no direct structural information is obtained, the structures and energetics of relatively simple gas-phase hydrates can generally be reliably computed by density functional theory (DFT). A number of theoretical studies on the hydration of

Received: January 21, 2012
Published: June 1, 2012

   dx.doi.org/10.1021/ic3001625 | *Inorg. Chem.* 2012, 51, 6603−6614

actinyl ions have been performed in the past decade.[10−29] As remarked above, the majority of the experimental studies indicate that the dominant coordination number for early AnO_2^{2+} in aqueous solution is five;[8,30−32] consequently, most theoretical effort has been directed toward penta-aquo complexes. Hydration of UO_2^{2+} is by far the most studied case. A critical review of theoretical studies of actinide chemistry in the gas-phase and in solution has been presented by Vallet et al.[24] Most theory studies concluded that five-coordination is the most favorable structure for the uranyl(VI) complexes in water, although some have suggested that five- and six-coordination are equally preferred.[18] From detailed computations of the equatorial coordination number of UO_2^{2+}, it is clear that the calculated coordination number is highly sensitive to several factors, including whether the computations are performed in the gas-phase or in solution, the accuracy of the gas-phase calculation, the solvation method, the inclusion of first/second solvation shells, and the inclusion of entropy effects.[20,21] Several previous theoretical studies report actinyl(V) and actinyl(VI) hydroxide gas-phase water complexes, including some of the cations studied in this work.[11,12,19,25−28,33]

Of particular interest in actinide chemistry, specifically actinyl chemistry, is the identification and comprehension of variations across the series, as from UO_2^+ to NpO_2^+ to PuO_2^+. An important result found in the course of the hydration studies reported here was the observation of O_2 addition to uranyl hydrates as a significant reaction pathway; these O_2 addition reactions were not observed for the corresponding neptunyl or plutonyl species. The gas-phase addition of O_2 to $UO_2^+\cdot(acetone)_{2,3}$ complexes has been reported;[34] a subsequent DFT study[35] characterized the $UO_2^+(O_2)(acetone)_{2,3}$ species as superoxo complexes, essentially with oxidation of U(V) to U(VI). Superoxo complexes were also produced by the addition of O_2 to uranyl(V) coordinated by acetone and water, as well as by dimethylsulfoxide and water.[36] These gas-phase results were particularly intriguing as Bakac and Espenson[37] had earlier proposed $U^{VI}O_2^{2+}(O_2^{\bullet-})$ as an intermediate in the copper-catalyzed oxidation of $U^VO_2^+$ to $U^{VI}O_2^{2+}$ in aqueous solution. Notably, $UO_2^+(O_2)(H_2O)_n$ complexes were evidently not previously observed in a gas phase study of the hydration of UO_2^+, despite the reported presence of $\sim 2 \times 10^{-7}$ Torr of O_2, this being a sufficient oxygen concentration to oxidize $UO(OH)^+$ to $UO_2(OH)^+$.[3] More recently, the superoxo cation complexes $UO_2^+(\eta^2\text{-}O_2)$ and $UO_2^+(\eta^2\text{-}O_2)(\eta^1\text{-}O_2)$ have been produced and characterized by IR spectroscopy and DFT.[38] The present results for reactions of actinyl(V) hydrates with oxygen serve to further illuminate the important issue of the formation of actinyl(VI) superoxides, particularly in the presence of water ligands.

The main goal of the DFT computations performed here was to provide insights into the experimental results. Accordingly, attention was focused on the sequential water-addition reactions of $AnO_2^+\cdot(H_2O)_n$ and $AnO_2(OH)^+\cdot(H_2O)_{n-1}$ (An = U, Np, and Pu, with n = 0−5) ions in the gas phase. The addition of O_2 to bare and hydrated UO_2^+ and NpO_2^+ ions was also studied by DFT to illuminate the nature of the observed uranyl hydrate−dioxygen adducts, as well as the underlying basis for the absence of such species in the case of neptunyl.

EXPERIMENTAL SECTION

Caution! *The ^{238}U, ^{237}Np, and ^{242}Pu isotopes used in this work are alpha-emitting radionuclides with half-lives of 4×10^9 years, 2×10^6 years, and 4×10^5 years, respectively. Special safety precautions must be followed when handling these isotopes. The experiments reported here were performed in a special radiological containment glovebox.*

The following stock acid solutions at Lawrence Berkeley National Laboratory (LBNL) were diluted to prepare the 180 μM actinyl solutions used for electrospray ionization (ESI): 177 mM $U^{VI}O_2(ClO_4)_2$ at pH = 0.6, 0.83 mM $Np^{VI}O_2(ClO_4)_2$ at pH = 1.6, and 0.70 mM $Pu^{VI}O_2(ClO_4)_2$ at pH = 1.6. The 180 μM uranyl solution had a measured pH = 3.9, reasonably close to the value of ∼3.6 expected on the basis of the ∼1000× dilution of the stock solution; NaOH was added to the 180 μM neptunyl and plutonyl solutions to obtain pH ≈ 4. To confirm that the ESI mass spectra were not sensitive to pH, solutions for all three actinyls were prepared with pH ≈ 2 by the addition of $HClO_4$, and with pH ≈ 6 by the addition of NaOH. The actinide isotopes (>99%) were U-238 (α-decay half-life = 4×10^9 years), Np-237 (α-decay half-life = 2×10^6 years), and Pu-242 (α-decay half-life = 4×10^5 years). All handling of these hazardous radionuclides was in a containment glovebox in a radiological laboratory. The ESI mass spectrometry experiments were performed using an Agilent 6340 quadrupole ion trap mass spectrometer (QIT/MS) with MS^n collision induced dissociation (CID) capabilities. A feature of the instrument is that ions in the trap can undergo ion−molecule reactions by applying a variable reaction delay time of up to 10 s; as no excitation is applied, observed reactions occur at the trap temperature of ∼300 K.[39] The source region of the QIT/MS is inside of a radiological-containment glovebox, as described in detail elsewhere.[40] In high resolution mode, the instrument has a detection range of 50−2200 m/z and a resolution of ∼0.25 m/z. Mass spectra were recorded in the positive ion accumulation and detection mode. Most spectra were taken with the following instrumental parameters: solution flow rate, 60 μL hr^{-1}; nebulizer gas pressure, 15 psi; capillary voltage and current, −4500 V, 14.648 nA; end plate voltage offset and current, −4500 V, 37.5 nA; dry gas flow rate, 5 L min^{-1}; dry gas temperature, 325 °C; capillary exit, 141.7 V; skimmer, 26.3 V; octopole 1 and 2 DC, 13.75 and 2.13 V; octopole RF amplitude, 58.3 Vpp; lens 1 and 2, −4.8 V and −65.5 V; trap drive, 216.8. High-purity nitrogen gas for nebulization and drying in the ion transfer capillary was supplied from the boil-off of a liquid nitrogen Dewar. As has been discussed elsewhere, the background water pressure in the ion trap is estimated as $\sim 10^{-6}$ Torr;[41] reproducibility of hydration rates confirms that the background water pressure in the trap remains constant to within <5%. The helium buffer gas pressure in the trap is constant at $\sim 10^{-4}$ Torr. The ion trap has been modified to allow for the introduction of reagent gases through a leak valve, including additional water in the present study.[40]

To provide confirmation of the uranyl results, particularly the hydration rates, and to obtain additional rates and reactions, independent uranyl studies were carried out at Instituto Tecnológico e Nuclear (ITN). The QIT/MS instrument at ITN is a Bruker HCT, which is very similar to the Agilent 6340 at LBNL, with comparable helium and water pressures in both ion traps; the results also suggest comparable O_2 pressures in both traps. The experimental conditions used at ITN are included as Supporting Information. Comparative hydration kinetics suggest that the water pressure is slightly greater in the ITN trap, which may be due to the use of a nitrogen generator, rather than the boil-off from liquid nitrogen, as the source for the ESI nebulizing and drying gas. The high capacity ion traps in both the Agilent instrument at LBNL and the Bruker instrument at ITN were manufactured and calibrated by Bruker, and both thus operate at essentially the same He bath gas pressure, which allows for reliable relative kinetics comparisons to be obtained for hydration reactions which involve third-body collisional cooling.

COMPUTATIONAL DETAILS

All quantum chemical calculations were performed within the framework of DFT using the B3LYP[42,43] hybrid functional and the Stuttgart small−core relativistic effective core potential (RECP) and associated basis sets for the actinide atoms.[44] The Stuttgart small-core RECP, the so-called SDD pseudopotential, replaces the 60 electrons in

dx.doi.org/10.1021/ic3001625 | Inorg. Chem. 2012, 51, 6603−6614

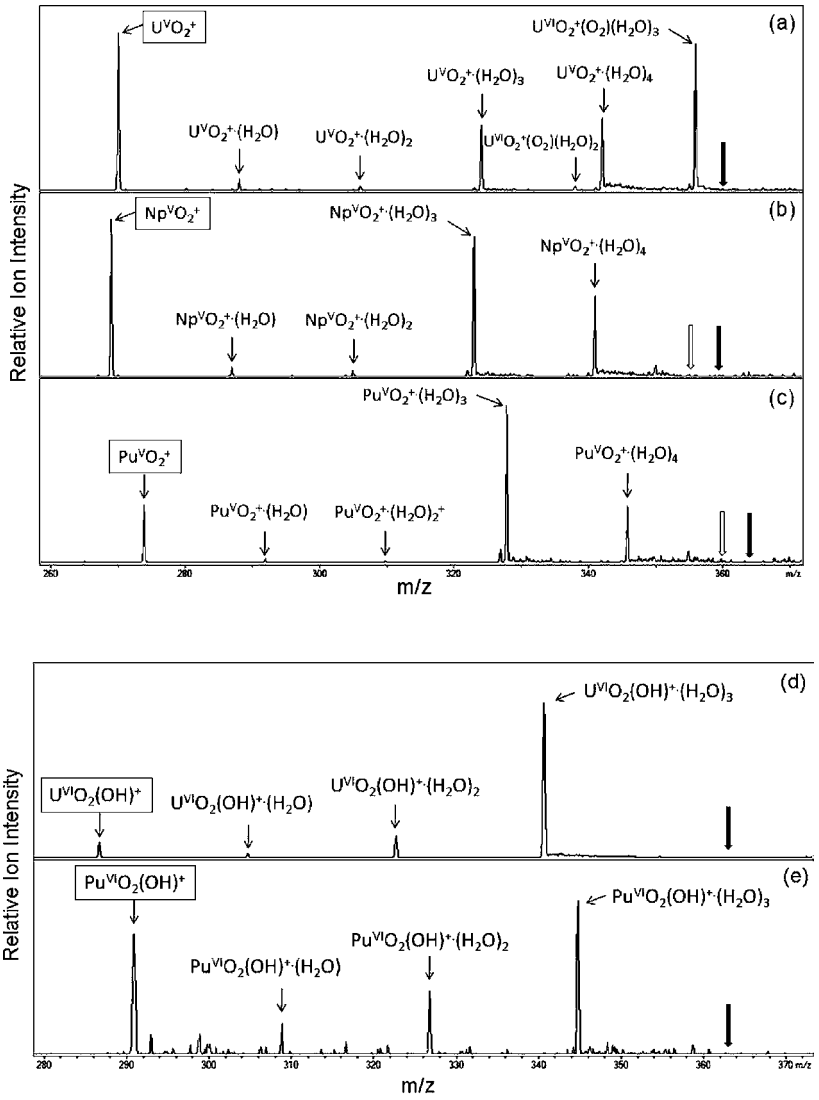

Figure 1. Top spectra: Products of isolated (a) $U^{V}O_2^+$, (b) $Np^{V}O_2^+$, and (c) $Pu^{V}O_2^+$ after a reaction time of 10 s. Bold arrows indicate where the nonobserved $An^{V}O_2^+\cdot(H_2O)_5$ hydrates would have appeared. The $U^{VI}O_2^+(O_2)(H_2O)_2$ and $U^{VI}O_2^+(O_2)(H_2O)_3$ species are evident in (a); open arrows in (b) and (c) indicate where $NpO_2^+(O_2)(H_2O)_3$ and $PuO_2^+(O_2)(H_2O)_3$ would have appeared. Bottom spectra: Products of isolated (d) $UO_2(OH)^+$ and (e) $PuO_2(OH)^+$ after a reaction time of 0.9 s. Bold arrows indicate where the nonobserved $AnO_2(OH)^+\cdot(H_2O)_4$ hydrates would have appeared. The several unassigned peaks in e reflect the minor intensity of $PuO_2(OH)^+$, which resulted in a low-intensity hydration mass spectrum with significant "noise".

the inner shells 1 through 4, leaving the explicit treatment of the $n = 5$ shell (5s, 5p, 5d, and 5f) and also the 6s, 6p, 6d, and 7s valence electrons. The choice of this level of theory (referred to as B3LYP/SDD) was based on the good performance found for similar calculations performed on the hydration of dipositive and monopositive actinyl and hydroxoactinyl ions.[19−21,25,26,28,45] The 6-311++G(d,p) basis sets were employed for the rest of the atoms.[46−48] These calculations were carried out with the Gaussian 09 package.[49] Ultrafine (99 590) pruned grids for numerical integration were employed in all of the computations.

The sequential hydration reactions were analyzed for six cations, namely, AnO_2^+ and $AnO_2(OH)^+$ for An = U, Np, and Pu. The geometry of the bare and hydrated cations, one to five water molecules for AnO_2^+ and one to four for $AnO_2(OH)^+$, was optimized without any symmetry restrictions. The lowest-energy structure is reported for each cation, along with some relevant high-energy structures. For each optimized stationary point, analytical frequencies were calculated to confirm that the optimized structure was a local minimum on the potential energy surface of the system, and to evaluate the zero-point vibrational energy (ZPVE) corrections to the electronic energies. All of the reported hydration energies include the ZPVE correction at 0 K (ΔE^0). The counterpoise correction was calculated to correct reaction energies for basis sets superposition errors.[50] In addition to the ΔE^0 values, the Gibbs free energy at 298 K is reported for each of the studied reactions. The accuracy of the ΔG^{298} values is necessarily somewhat limited by the use of the harmonic oscillator approximation to treat nuclear motion. Spin−orbit effects were not treated explicitly in this study. Spin−orbit effects are expected to be especially important for most of the cations studied here, as they exhibit open-shell ground states. However, these contributions have been shown to remain invariant with the addition of water molecules and therefore are not expected to significantly affect the sequential hydration energies.[25]

In order to confirm that the used level of theory correctly identifies the lowest-energy spin state of the systems, two or more spin states were considered for each of the bare cations studied here. Exploratory calculations on the first and second hydrates of all the studied cations were performed in order to establish whether the addition of coordinating water molecules could change the lowest energy spin state of the ions. In all cases, it was found that the lowest energy spin state of the hydrates is the same as that of the corresponding bare

dx.doi.org/10.1021/ic3001625 | Inorg. Chem. 2012, 51, 6603−6614

cations. Therefore, only the lowest-energy spin states of the bare cations were considered when studying the successive hydrates, namely, doublet spin state for UO_2^+, triplet for NpO_2^+, quartet for PuO_2^+, singlet for $UO_2(OH)^+$, doublet for $NpO_2(OH)^+$, and triplet for $PuO_2(OH)^+$. Calculations were carried out using spin-unrestricted methods. No appreciable spin contamination was found in any of these species.

The geometrical and energetic properties of the dioxygen complexes $UO_2^+(O_2)(H_2O)_n$ and $NpO_2^+(O_2)(H_2O)_n$ for $n = 0-3$ were performed at the same level of theory (B3LYP/SDD), and the energetics associated with the O_2 addition to the different hydrates is reported. It was considered that computations for these two systems would suffice to understand the distinctive nature of uranyl; accordingly, computations were not performed for $PuO_2^+(O_2)(H_2O)$. Two possible dioxygen coordination modes were considered, i.e., end-on (η^1) and side-on (η^2). The doublet and quartet spin states were considered in the case of $UO_2^+(O_2)(H_2O)_n$ and the singlet, triplet, and quintet states for the corresponding neptunyl cations. The broken-symmetry approach[51−54] was used to investigate the geometrical and energetic properties of the (open-shell) singlet η^1-$NpO_2^+(O_2)(H_2O)_n$ cation.

The charge distribution was analyzed using Natural Population Analysis (NPA)[55] as implemented in the Gaussian 09 package (NBO version 3.1).

RESULTS AND DISCUSSION

Whereas the neptunyl and plutonyl experiments were all performed at LBNL, uranyl experiments were performed at both LBNL and ITN, with essentially the same results. Obtaining duplicate results for uranyl was particularly important for the comparative hydration kinetics presented below in view of a significant discrepancy between the results obtained in this work and those reported previously.[3]

ESI-MS of Uranyl, Neptunyl, and Plutonyl. ESI of aqueous solutions of $An^{VI}O_2(ClO_4)_2$ (An = U, Np, Pu) generates both pentavalent and hexavalent monopositive gas-phase actinyl ions: $U^VO_2^+$, $Np^VO_2^+$, $Pu^VO_2^+$, $U^{VI}O_2(OH)^+$, and $Pu^{VI}O_2(OH)^+$; similar ESI mass spectra were obtained over a pH range from ~2 to ~6. Hydrates of dipositive AnO_2^{2+} did not appear in the ESI mass spectra; all three dipositive AnO_2^{2+} (An = U, Np, Pu) had previously been transferred from solution to gas in complexes with strong Lewis base ligands such as dimethylformamide (DMF) in the gaseous $AnO_2^{2+}\cdot(DMF)_4$ complex ions.[56] Evidently, ligands which are better electron donors than water are required to effectively stabilize dipositive actinyls from solution to the gas phase under our experimental conditions.

The primary disparity among the actinyls apparent in the ESI mass spectra is the appearance of substantial $U^{VI}O_2(OH)^+$ (~60% relative to UO_2^+), minor $Pu^{VI}O_2(OH)^+$ (~5% relative to PuO_2^+), and no detectable $Np^{VI}O_2(OH)^+$ (to an estimated detection limit of <3% relative to NpO_2^+). The overwhelmingly dominant process in ESI of $Np^{VI}O_2^{2+}$ and $Pu^{VI}O_2^{2+}$ is charge and oxidation state reduction to $An^VO_2^+$. In contrast, a significant product from ESI of $U^{VI}O_2^{2+}$ is $U^{VI}O_2(OH)^+$, in which charge-reduction has occurred but the hexavalent oxidation state is retained by hydrolysis to produce the hydroxide. ESI from a predominantly D_2O (>99%) solution resulted in almost exclusively $UO_2(OH)^+$ rather than $UO_2(OD)^+$; this result does not reveal whether hydrolysis occurs by reaction with background H_2O in the gas phase, or rather whether $UO_2(OD)^+$ is produced during ESI and subsequently undergoes gas-phase hydroxyl-exchange with background H_2O. Hay et al.[13] have computed that the gas-phase hydrolysis of UO_2^{2+} to $UO_2(OH)^+$ ($+H_3O^+$) is thermodynamically favorable, but the kinetics for this process are unknown. Regardless of the mechanism of hydroxide formation, the relative abundances, $U^{VI}O_2(OH)^+ \gg Pu^{VI}O_2(OH)^+ > Np^{VI}O_2(OH)^+$ (the last of these was not observed), are consistent with the relative stabilities of the hexavalent actinide oxidation states, as indicted by the standard reduction potentials for $An^{VI}O_2^{2+} \rightarrow An^VO_2^+$: 0.09 V for $UO_2^{2+} \ll 0.94$ V for $PuO_2^{2+} < 1.16$ V for NpO_2^{2+}.[57]

Hydration of AnO_2^+ (An = U, Np, Pu). The AnO_2^+ ions were isolated and exposed to water present at a constant but indeterminate ($\sim10^{-6}$ Torr) pressure in the ion trap.[41] Third body collisions with the helium buffer gas serve to collisionally cool nascent hydrates, as has been demonstrated previously by a nearly linear dependence of hydration rates on helium pressure.[41] Because measured hydration rates under these conditions are highly dependent on third-body collisions, it is not valid to report pseudo-first-order rate constants for hydration; these rates would be negligible in the absence of a high pressure of cooling gas, $\sim10^{-4}$ Torr of helium in the present experiments. However, it is appropriate to report relative hydration rates obtained under comparable conditions of both water pressure and helium pressure.

Representative hydration results are shown in Figure 1 as mass spectra acquired for isolated UO_2^+, NpO_2^+, and PuO_2^+ after reaction with background gases in the trap for 10 s, the maximum accessible reaction time using the "block voltage scan delay" option in the QIT/MS software. It is apparent in Figure 1 that hydration of all three AnO_2^+ terminates at the tetrahydrate, $AnO_2^+\cdot(H_2O)_4$. Additional water vapor was added to the trap through a leak valve; increasing the water pressure by approximately a factor of 2 accordingly increased the yields of the $AnO_2^+\cdot(H_2O)_4$ hydrate ions but resulted in no detectable pentahydrates, $AnO_2^+\cdot(H_2O)_5$. Previous hydration studies of ligated monopositive metal ions under these same experimental conditions led to the conclusion that the terminal observed hydrates correspond to the maximum extent of inner-sphere hydration in the gas-phase complexes; the addition of second sphere water molecules is not observed under these conditions.[41]

Other features evident in Figure 1 include the appearance of uranyl oxygen adducts and differences between the rates of hydration among the three AnO_2^+ ions. These aspects are discussed below.

The most relevant optimized parameters of the ground-state (GS) $AnO_2^+\cdot(H_2O)_n$ (An = U, Np, and Pu, $n = 0-5$) structures and some relevant higher-energy isomers are presented in Table 1. In the chemical formulas of the hydrates, water molecules in the second solvation shell are shown in italics. In the discussion, tables, and figures, O_{yl} is used to designate an axial actinyl oxygen atom, and O_w is used to designate an oxygen atom in an equatorial water ligand. The geometrical structures of $AnO_2^+\cdot(H_2O)_4(H_2O)$ GS and the $AnO_2^+\cdot(H_2O)_5$ higher-energy isomer are shown in Figure 2. For all three AnO_2^+ cations, the addition of water induces a lengthening of actinyl bond length, by ca. 0.04 Å from $n = 0$ to $n = 5$. The actinyl−water distance increases on going from $AnO_2^+\cdot(H_2O)$ to $AnO_2^+\cdot(H_2O)_4$ by between 0.06 and 0.09 Å, depending on the actinide. At the level of theory used in this work, the lowest-energy pentahydrates are obtained when the fifth water molecule is placed in the second coordination shell, forming hydrogen bonds with two water molecules from the first coordination shell, designated as $AnO_2^+\cdot(H_2O)_4(H_2O)$, as shown in Figure 2. These isomers, however, are followed

dx.doi.org/10.1021/ic3001625 | Inorg. Chem. 2012, 51, 6603−6614

Table 1. Computed Bond Distances of the Ground-State $AnO_2^+\cdot(H_2O)_n$, n = 0−5, Structures and the Pentacoordinated $AnO_2^+\cdot(H_2O)_5$ Isomers[a]

	An−O_{yl}	An−O_w
UO_2^+	1.76	
NpO_2^+	1.74	
PuO_2^+	1.73	
$UO_2^+\cdot(H_2O)$	1.77	2.48
$NpO_2^+\cdot(H_2O)$	1.75	2.45
$PuO_2^+\cdot(H_2O)$	1.73	2.44
$UO_2^+\cdot(H_2O)_2$	1.79	2.50
$NpO_2^+\cdot(H_2O)_2$	1.76	2.48
$PuO_2^+\cdot(H_2O)_2$	1.75	2.46
$UO_2^+\cdot(H_2O)_3$	1.79	2.50
$NpO_2^+\cdot(H_2O)_3$	1.77	2.50
$PuO_2^+\cdot(H_2O)_3$	1.76	2.49
$UO_2^+\cdot(H_2O)_4$	1.80	2.54
$NpO_2^+\cdot(H_2O)_4$	1.78	2.54
$PuO_2^+\cdot(H_2O)_4$	1.77	2.53
$UO_2^+\cdot(H_2O)_4(H_2O)$[b]	1.80, 1.82	2.52−2.53
$NpO_2^+\cdot(H_2O)_4(H_2O)$[b]	1.78, 1.80	2.52−2.53
$PuO_2^+\cdot(H_2O)_4(H_2O)$[b]	1.77, 1.78	2.51−2.52
$UO_2^+\cdot(H_2O)_5$	1.80	2.58−2.61
$NpO_2^+\cdot(H_2O)_5$	1.79	2.59−2.60
$PuO_2^+\cdot(H_2O)_5$	1.77	2.58−2.62

[a]In angstroms. Ranges of An−O_w distances are given for the fifth hydrate. [b]Ground-state structures for the fifth hydrate. These structures are characterized by the presence of two different An−O_{yl} bond distances. Experimental values (in Å) for $NpO_2^+\cdot(H_2O)_5$: Np−O_{yl} bond, 1.83[30] and 1.83;[69] Np−O_w bond, 2.50[30] and 2.52.[69] Experimental values (in Å) for $PuO_2^+\cdot(H_2O)_5$: Pu−O_{yl} bond, 1.81; Pu−O_w bond, 2.47.[69]

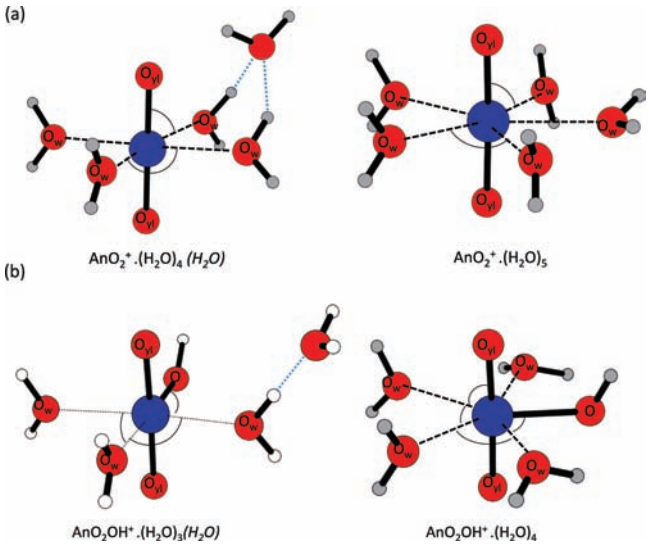

Figure 2. (a) Geometric structures of pentahydrated AnO_2^+ ions. $AnO_2^+\cdot(H_2O)_4(H_2O)$ is the ground-state structure, whereas $AnO_2^+\cdot(H_2O)_5$ is higher in energy. (b) Lowest-energy optimized structures of tetrahydrated AnO_2OH^+ ions. $AnO_2OH^+\cdot(H_2O)_3(H_2O)$ is the ground-state structure, whereas $AnO_2OH^+\cdot(H_2O)_4$ is higher in energy. Italics denote water molecules in the second solvation shell. The most relevant geometric parameters are reported in Tables 1 and 3, respectively.

very closely in energy by the corresponding inner-sphere pentacoordinate isomers, $AnO_2^+\cdot(H_2O)_5$ (Figure 2).

As shown in Table 1, for the series of complexes $AnO_2^+\cdot(H_2O)_n$ (n = 0−4), the actinyl bond lengths show a slight contraction (ca. 0.03 Å) upon progressing along the series, from U to Pu. This trend is in agreement with previous theoretical,[13,20,21,24,28] and experimental,[30,58] studies that show a slight decrease in the An−O_{yl} bond length across the actinide series, together with a decrease in symmetric and antisymmetric O═An═O stretching frequencies.[13,58] Recent experimental studies have confirmed that the An−O bond strength diminishes across the series,[59] which is the expected trend on the basis of the decrease of the stretching frequency. The actinyl bond, therefore, becomes both shorter and weaker along the series.

According to experimental estimations, the effective metal charge of the actinyl(VI) cations in aqueous solutions diminishes on going from U to Pu.[60] Our calculations show the same trend in the case of actinyl(V) ions (Table S1). In particular, the computed NPA values for the tetrahydrates diminish from 1.70 for $UO_2^+\cdot(H_2O)_4$ to 1.45 for $PuO_2^+\cdot(H_2O)_4$. The computed NPA value for $NpO_2^+\cdot(H_2O)_4$ (1.59) is lower than the experimental effective charge on Np in NpO_2^+ in the aqueous phase, 2.2 ± 0.1,[60] which was obtained using a modified Born equation and stability constants. The actinide natural charges and orbital populations of the three bare cations are included as Supporting Information (Table S2).

The computed reaction energies at 0 K and Gibbs free energies at 298 K for all of the sequential hydration reactions are summarized in Table 2. The sequential hydration energies are in all cases exothermic and show a monotonic decrease in magnitude with an increase in the number of coordinated water molecules. The hydration energies change from −134 kJ mol^{-1} for the formation of the first hydrate, $UO_2^+\cdot(H_2O)$, to −83 kJ mol^{-1} for the formation of the tetrahydrate, $UO_2^+\cdot(H_2O)_4$. The first two hydration energies are practically identical for all three studied cations (UO_2^+, NpO_2^+, and PuO_2^+), whereas there is a slight, but systematic, decrease in the magnitudes of the hydration energies (up to 9 kJ mol^{-1}) on going from uranium to plutonium, for the addition of the third and fourth water molecules. The variations in the computed hydration energies are in all cases consistent with the decrease of the effective charge on the metal center (Supporting Information, Tables S1 and S2).

The ground-state pentahydrates are obtained when the fifth water molecule is placed in the second coordination shell, $AnO_2^+\cdot(H_2O)_4(H_2O)$, with an exothermicity of almost 50 kJ mol^{-1}. The $AnO_2^+\cdot(H_2O)_5$ isomers with five inner-sphere water molecules were calculated to be very close in energy to the GS structures (i.e., within 11 kJ mol^{-1}). Calculations show, therefore, that the additions of a fifth water molecule to the $AnO_2^+\cdot(H_2O)_4$ complexes are exothermic. However, the computed ΔG^{298} values are considerably less favorable due to the unfavorable entropy of association (Table 2). In particular, the fifth hydration is practically ergoneutral ($\Delta G \sim 0$). Moreover, due to differences in the entropy of reaction, the ΔG^{298} of formation of the pentacoordinated $AnO_2^+\cdot(H_2O)_5$ and tetracoordinated $AnO_2^+\cdot(H_2O)_4(H_2O)$ isomers are essentially the same. A complete table including ΔH^{298} and ΔS^{298} values for all of the reported reactions is in the Supporting Information (Table S3). In a previous study, we discussed whether the exothermicity, ΔH^{298}, or the exoergicity, ΔG^{298}, should be considered for the conditions used in the experiments performed here.[41] It was concluded that under

dx.doi.org/10.1021/ic3001625 | Inorg. Chem. 2012, 51, 6603−6614

Table 2. Computed Energy (ΔE^0), and Gibbs Free Energy (ΔG^{298}) Changes for the AnO_2^+ and $AnO_2(OH)^+$ Hydration Reactions[a]

reaction	UO_2^+	NpO_2^+	PuO_2^+	UO_2OH^+	$NpO_2(OH)^+$	$PuO_2(OH)^+$
			$n = 1$			
ΔE^0	−134	−134	−133	−143 [−143][b]	−141	−136
ΔG^{298}	−109	−104	−120	−110	−104	−99
			$n = 2$			
ΔE^0	−117	−118	−118	−123 [−124][b]	−123	−118
ΔG^{298}	−81	−82	−82	−83	−88	−83
			$n = 3$			
ΔE^0	−108	−106	−104	−93	−94	−87
ΔG^{298}	−72	−70	−68	−54	−56	−49
			$n = 4$			
ΔE^0	−83	−79	−74	−55 (−44) [−46][b]	−54 (−40)	−53 (−31)
ΔG^{298}	−45	−46	−38	−29 (−5)	−23 (−2)	−22 (5)
			$n = 5$			
ΔE^0	−48 (−37)	−45 (−34)	−44 (−33)			
ΔG^{298}	−6 (−7)	−2 (2)	−3 (0)			

[a]In kJ·mol^{-1}. The reactions correspond to successive hydration reactions: $AnO_2^+\cdot(H_2O)_{n-1} + H_2O \rightarrow AnO_2^+\cdot(H_2O)_n$ and $AnO_2OH^+\cdot(H_2O)_{n-1} + H_2O \rightarrow AnO_2OH^+\cdot(H_2O)_n$, respectively. Values in parentheses correspond to higher-energy inner-sphere species. [b]In brackets: B3LYP/SDD (U)-aug-cc-pVDZ(O,H).[27]

the conditions used here—specifically a pressure of ∼10^{-4} Torr—third-body collisions are crucial to stabilizing the hydration products, and the Gibbs free energy changes are accordingly more relevant than hydration energies or enthalpies.[41] The absence of pentahydrates in the experiments is in accord with the computed free energies for the addition of the fifth water molecule. Although it is not functional to define an equilibrium constant for reactions corresponding to the association of water to cations present at very low and unknown concentrations, it can be inferred that under the low-pressure conditions of these experiments—i.e., ∼10^{-6} Torr H_2O—the hydration free energy must be adequately negative to provide a sufficiently favorable effective "equilibrium constant" for hydration to be observed. It should be noted that as the free energies are nearly the same for the addition of the fifth water in the inner-sphere or outer sphere, the experimental results—i.e., termination at the tetrahydrate—do not directly distinguish between inner-sphere and outer-sphere coordination but do demonstrate that the maximum inner-sphere coordination is by four water molecules in the gas phase.

In summary, our computations indicate that at the present level of theory the tetracoordinated isomer, $AnO_2^+\cdot(H_2O)_4(H_2O)$, is slightly favored energetically. The calculated Gibbs free energy of hydration for both the tetra- and pentacoordinated isomers is essentially the same. The key point of the computational results in relation to the experiments performed here is that the calculated Gibbs free energy of formation for the pentahydrated actinyl(V) cations, both tetra- and pentacoordinated, is essentially unfavorable at low water pressures such as ∼10^{-6} Torr employed in the experiments; the DFT results effectively explain the absence of pentahydrates.

Hydration of $AnO_2(OH)^+$ (An = U, Np, Pu). The gas-phase hydration behaviors of $UO_2(OH)^+$ and $PuO_2(OH)^+$ were examined, with the key results shown in Figure 1. In contrast to the AnO_2^+ ions, these actinyl hydroxides add only three water molecules with hydration terminating at $AnO_2(OH)^+\cdot(H_2O)_3$ for both An = U and Pu. Increasing the reaction time resulted in an increase in the abundance of the terminal trihydrate, but not in the appearance of any detectable $AnO_2(OH)^+\cdot(H_2O)_4$. As discussed above for the AnO_2^+, the interpretation of this result, substantiated by DFT results as discussed below, is that the maximum inner-sphere hydration of the $AnO_2(OH)^+$ is three and that the addition of outer-sphere water molecules is not observed under these conditions. The hydration rates are discussed below.

Despite the fact that $NpO_2(OH)^+$ was not observed experimentally, all three $AnO_2(OH)^+$ ions were computationally studied. The most relevant optimized parameters of the ground-state $AnO_2(OH)^+$ (An = U, Np, and Pu) ions and their hydrates (n = 0−4) are collected in Table 3; the geometrical structures of the $AnO_2(OH)^+(H_2O)_3(H_2O)$ GS and the higher energy $AnO_2OH^+(H_2O)_4$ isomers are shown in Figure 2. Our calculations indicate that the lowest-energy structure for the tetrahydrate is obtained when the fourth water molecule is

Table 3. Computed Bond Distances for the Ground-State $AnO_2(OH)^+\cdot(H_2O)_n$, n = 0−4, Structures[a]

	An−O_{yl}	An−OH	An−O_w
$UO_2(OH)^+$	1.74	2.01	
$NpO_2(OH)^+$	1.73	2.01	
$PuO_2(OH)^+$	1.72	2.02	
$UO_2(OH)^+\cdot(H_2O)$	1.76	2.03	2.44
$NpO_2(OH)^+\cdot(H_2O)$	1.74	2.02	2.43
$PuO_2(OH)^+\cdot(H_2O)$	1.73	2.03	2.42
$UO_2(OH)^+\cdot(H_2O)_2$	1.76	2.05	2.49
$NpO_2(OH)^+\cdot(H_2O)_2$	1.74	2.04	2.47
$PuO_2(OH)^+\cdot(H_2O)_2$	1.73	2.05	2.47
$UO_2(OH)^+\cdot(H_2O)_3$	1.77	2.07	2.50−2.54
$NpO_2(OH)^+\cdot(H_2O)_3$	1.75	2.07	2.49−2.52
$PuO_2(OH)^+\cdot(H_2O)_3$	1.73	2.07	2.48−2.53
$UO_2(OH)^+\cdot(H_2O)_3H_2O$[b]	1.78	2.08	2.43−2.55
$NpO_2(OH)^+\cdot(H_2O)_3H_2O$[b]	1.76	2.07	2.42−2.53
$PuO_2(OH)^+\cdot(H_2O)_3H_2O$[b]	1.74	2.08	2.42−2.54
$UO_2(OH)^+\cdot(H_2O)_4$	1.77	2.13	2.56−2.58
$NpO_2(OH)^+\cdot(H_2O)_4$	1.75	2.13	2.56−2.57
$PuO_2(OH)^+\cdot(H_2O)_4$	1.73	2.12	2.54−2.56

[a]In angstroms. Ranges of An−O_w distances are given for the third and fourth hydrates. [b]Ground-state structure for the fourth hydrate.

dx.doi.org/10.1021/ic3001625 | Inorg. Chem. 2012, 51, 6603−6614

added in the second solvation shell. Several isomers with three water molecules in the inner-shell and the fourth interacting in different coordination motifs in the second shell were found to be practically degenerate in energy with the GS structure; these structures are included as Supporting Information (Figures S1 to S3). The lowest-energy isomer with four water molecules in the inner sphere is higher in energy than the GS by 9 kJ mol^{-1} for $UO_2(OH)^+$, by 22 kJ mol^{-1} for $NpO_2(OH)^+$, and by 18 kJ mol^{-1} for $PuO_2(OH)^+$. The incremental addition of water molecules to the complexes results in essentially no change in the An−O_{yl} axial bonds. The An−OH bond distances are more sensitive to the effect of the addition of water molecules. The increase in the An−OH bond distances on going from the bare $AnO_2(OH)^+$ cations to the $AnO_2(OH)^+\cdot(H_2O)_3$ trihydrates is about 0.06 Å (see Table 3).

The successive hydration energies for the three studied $AnO_2(OH)^+$ cations are provided in Table 2, together with the Gibbs free energy changes at 298 K. A complete table containing ΔH^{298} and ΔS^{298} values is included as Supporting Information (Table S3). The energies for the addition of the first two water molecules to the $AnO_2(OH)^+$ and AnO_2^+ ions are quite similar. As observed for the actinyl ions, a slight decrease in the magnitude of the hydration energies was found in the actinyl hydroxide cations on going through the series, from U to Pu. Again, the computed Gibbs free energy changes for successive hydrations are notably less favorable than the energy changes, due to the unfavorable entropy for gas-phase association processes. The fourth hydration is exoergic by ∼25 kJ mol^{-1} for the ground-state structure and practically ergoneutral in the case of the isomer with four inner-sphere water molecules.

The addition of a fourth outer-sphere water to $UO_2(OH)^+$ is computed to be exoergic by −29 kJ mol^{-1}, yet $UO_2(OH)^+\cdot(H_2O)_4$ is not observed in the experiments. The addition of the fourth inner-sphere water to PuO_2^+ is computed to be exoergic by −38 kJ mol^{-1}, and $PuO_2^+\cdot(H_2O)_4$ is experimentally observed. The free energy difference of −29 kJ mol versus −38 kJ mol corresponds to an increase in the "equilibrium constant" by ∼40× at 298 K. However, the error in the DFT free energies is sufficiently large—e.g., at least ±5 kJ mol^{-1}—that the difference could be substantially greater than 9 kJ mol^{-1}.

Comparative Hydration Kinetics: AnO_2^+ versus $AnO_2(OH)^+$. The primary hydration rates corresponding to eq 2 were measured for the five actinyl ions which could be isolated, $I^+ = UO_2^+$, NpO_2^+, PuO_2^+, $UO_2(OH)^+$, or $PuO_2(OH)^+$.

$$I^+ + H_2O \rightarrow I^+\cdot(H_2O) \quad (2)$$

As the water pressure in the trap is constant, the kinetics for eq 2 are pseudo-first-order, as given by eqs 3a and 3b.

$$d[I^+]/dt = k[H_2O][I^+] = k'[I^+] \quad (3a)$$

$$\ln\{[I^+]/[I^+]_0\} = -k't \quad (3b)$$

The values of k' were obtained from the slope of the log of the actinyl ion decay versus time (an example is shown in Figure S4). Because the water pressure, as well as the helium pressure, was held constant for all kinetics determinations, the measured rates directly provide comparative kinetics. Rates for uranyl species were measured at ITN as well as at LBNL, to confirm and extend the kinetics comparisons. Measured rates are given in the Supporting Information (Table S4). For comparative purposes, the following relative rates are normalized to the fastest, so that $UO_2(OH)^+$ in the present work is designated as 100%. The relative rates in italics were determined at ITN (uncertainties are given in parentheses); values from Gresham et al.[3] are in brackets:

$$UO_2(OH)^+/100;\ \textit{100};\ [63] > PuO_2(OH)^+/40(18) \gg PuO_2^+/5.0(0.9) \approx UO_2^+/3.9(0.6);\ \textit{3.5(0.5)};\ [100] \approx NpO_2^+/3.5(0.5)$$

As the rates depend on the extent of third body collisional stabilization, these relative rates will not necessarily be observed under conditions where the pressure of the cooling gas is significantly higher or lower. Given the magnitudes of the assigned uncertainties, differences in the rates between the two $AnO_2(OH)^+$ ions, as well as among the three AnO_2^+'s, are considered minor. The particularly large uncertainty for $PuO_2(OH)^+$ is attributed to the very low abundance of that reactant ion (see Figure 1e). As is evident from the comparison of the spectra in Figure 1, as well as the measured rates reported above, the $AnO_2(OH)^+$ ions hydrate much more efficiently than do the AnO_2^+ ions, with the rate of hydration of $UO_2(OH)^+$ more than an order of magnitude faster than that of UO_2^+, as determined at both LBNL (26× faster) and ITN (29× faster). In contrast to the present results, Gresham et al.[3] reported that the hydration rate for $UO_2(OH)^+$ is somewhat slower than that for UO_2^+. These previous kinetics results were obtained under similar conditions to those employed here, in an ion trap mass spectrometer with a helium pressure of ∼10^{-4} Torr and a water pressure of ∼10^{-6} Torr. The origins of the disparity are not obvious but may be related to the adaptive simulated annealing (ASA) methodology employed in the previous work to model kinetics and derive rate constants.[3] The pseudo-first-order kinetics were directly determined in the present work (see Figure S4); furthermore, comparison of the extent of depletion of UO_2^+ after 10 s (Figure 1a) with that of $UO_2(OH)^+$ after 0.9 s (Figure 1d), at constant water pressure, clearly reveals that hydration of the latter is much faster. As has been discussed by Böhme and co-workers for association reactions of metal ions with water,[61,62] the comparative kinetics obtained in the present work—i.e., substantially faster hydration for $UO_2(OH)^+$ versus UO_2^+—is attributed to the additional hydroxyl vibrational degrees of freedom in the hot $\{AnO_2(OH)^+\cdot(H_2O)\}^*$ product as compared with $\{AnO_2^+\cdot(H_2O)\}^*$. The ability of nascent hydroxyl hydrates to more effectively dissipate the hydration energy results in longer-lived association complexes which have a greater opportunity for third-body collisional cooling prior to dissociation.

It was also possible to obtain the following relative sequential hydration rates for $UO_2(OH)^+$ and UO_2^+ at LBNL and/or ITN (ITN values are in italics; uncertainties are in parentheses); values from Gresham et al.[3] are in brackets:

dx.doi.org/10.1021/ic3001625 | Inorg. Chem. 2012, 51, 6603−6614

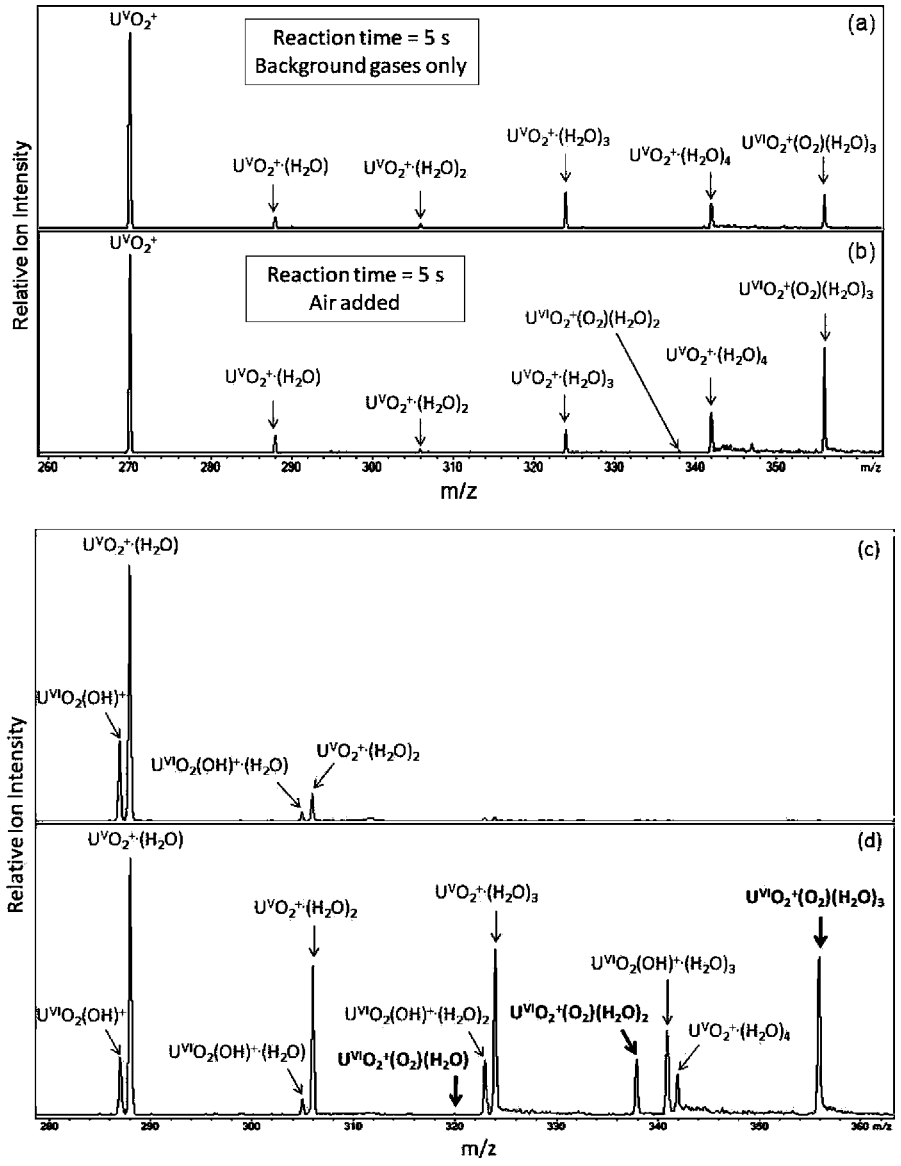

Figure 3. Top spectra: Reaction of isolated UO_2^+ for 5 s, (a) with background gases and (b) after the addition of air to the ion trap. The same experiment performed with NpO_2^+ and PuO_2^+ resulted in only the hydrates, no O_2-addition products. Bottom spectra: Reaction of isolated $UO_2^+\cdot(H_2O)$ and $UO_2(OH)^+$ with background gases and added air for (c) no applied reaction time and (d) a reaction time of 0.5 s. The product spectrum d shows O_2 addition to $UO_2^+\cdot(H_2O)_2$ and $UO_2^+\cdot(H_2O)_3$ but not to $UO_2^+\cdot(H_2O)$. The appearance of products in spectrum (c) without any applied reaction time reflects an inherent time delay of ~70 ms associated with ion isolation. The "soft ESI" conditions used to enhance the yield of $UO_2^+\cdot(H_2O)$ are described in the Supporting Information (Figure S5).

$UO_2(OH)^+\cdot(H_2O)/100$; *100*; [100]

> $UO_2(OH)^+\cdot(H_2O)_2/40(18)$; *45(3)*; [31]

> $UO_2(OH)^+/20(2)$; *22(2)*; [27]

$UO_2^+\cdot(H_2O)/100$; [100]

≫ $UO_2^+/4.4(0.4)$; [20]

There is good agreement between the LBNL and ITN relative rates for $UO_2(OH)^+\cdot(H_2O)_n$, and also reasonable agreement with those reported by Gresham et al.[3] The water ligand in $UO_2(OH)^+\cdot(H_2O)$ apparently provides additional stabilization of hot product $\{UO_2(OH)^+\cdot(H_2O)_2\}^*$ to enable collisional cooling and enhance hydration efficiency. In accord with evaluations of Böhme and co-workers,[61,62] the decreasing thermodynamic benefit of the addition of the third water ligand offsets the additional degrees of freedom in $\{UO_2(OH)^+\cdot(H_2O)_3\}^*$ (see Table 2). The same general rate trend for the corresponding $PuO_2(OH)^+\cdot(H_2O)_n$ (n = 0, 1, 2) is deduced from the similar hydrate abundances in Figure 1d and e.

The above comparative sequential hydration rates obtained for UO_2^+ and $UO_2^+\cdot(H_2O)$ are in qualitative accord with relative rate constants obtained by Gresham et al.[3] The hydration rate for bare UO_2^+, although thermodynamically the most favorable, is much lower than that for the hydration of $UO_2^+\cdot(H_2O)$, reflecting insufficient degrees of freedom for energy dissipation in the stiff bare uranyl ion. The addition of a single water ligand renders the hydration of $UO_2^+\cdot(H_2O)$ much more efficient. There is a correspondence between the results for UO_2^+ and $UO_2(OH)^+$, for both of which the monohydrate adds water much more efficiently than does the bare ion, which

dx.doi.org/10.1021/ic3001625 | Inorg. Chem. 2012, 51, 6603−6614

is attributed to the presence of a single water ligand providing additional vibrational excitation modes for energy dissipation and collisional cooling prior to dissociation.[61,62]

Oxygen Addition to $AnO_2^+(H_2O)_n$: Uranyl versus Neptunyl. A striking result evident in Figure 1a is the appearance of an intense peak corresponding to $UO_2^+(O_2)(H_2O)_3$ and a minor peak corresponding to $UO_2^+(O_2)(H_2O)_2$. No such O_2-addition products were observed in the corresponding spectra for NpO_2^+ or PuO_2^+, as is evident in Figure 1b and c. The dioxygen addition products are attributed to a reaction with background O_2 in the ion trap. As confirmation, the addition of air into the trap resulted in a substantial increase in the relative intensity of the peak corresponding to $UO_2^+(O_2)(H_2O)_3$, as seen in Figure 3b. A similar addition of air to the trap after isolation of NpO_2^+ and PuO_2^+ did not result in any detectable O_2-addition products. To confirm the minor $UO_2^+(O_2)(H_2O)_2$ product evident in Figures 1a and 3b, the ESI yield of $UO_2^+\cdot(H_2O)$ was optimized using the instrumental parameters given in the caption to Figure S5. As is evident in Figure 3d (and Figure S5), both $UO_2^+(O_2)(H_2O)_2$ and $UO_2^+(O_2)(H_2O)_3$ are significant products. It is also apparent from Figure 3d that $UO_2^+(O_2)(H_2O)$ is not produced: O_2 addition evidently occurs only for uranyl(V) dihydrate and trihydrate.

As O_2 addition to other UO_2^+ complexes has been previously reported,[34−36,38] an observation of particular interest in the present study is the difference between uranyl(V) hydrates, which add O_2, versus neptunyl(V) and plutonyl(V) hydrates, which do not. DFT computations were performed to understand the nature of the $UO_2^+(O_2)(H_2O)_n$ products and why O_2-addition products were not similarly produced for NpO_2^+; these computations were not performed for PuO_2^+, as its behavior is similar to NpO_2. Several initial structures were considered for each of the cations investigated, taking into account two possible O_2-coordination modes, i.e., end-on (η^1) and side-on (η^2). Different possible spin multiplicities (doublet and quartet for $UO_2^+(O_2)(H_2O)_n$; singlet, triplet, and quintet for $NpO_2^+(O_2)(H_2O)_n$) were considered for each of the coordination modes.

The geometrical parameters of the lowest-energy structures of the $UO_2(O_2)^+$ cation and its hydrates are shown in Figure 4; the energy changes together with the free energy changes for the addition of O_2 to the bare and hydrated cations are presented in Table 4 (enthalpy and entropy changes are included as Supporting Information, Table S5). Our computations indicate that O_2 binds to UO_2^+ in a side-on (η^2) configuration for the $UO_2^+(O_2)$ bare cation and its hydrates, in analogy with previous results for other UO_2^+ complexes.[35,36,38] All of the $UO_2^+(\eta^2\text{-}O_2)(H_2O)_n$ structures are in the doublet ground-spin state, and the O−O bond lengths (ca.1.30 Å) are those of a superoxo complex in which uranium(V) has been oxidized to uranium(VI).[35,38] The dioxygen binding energies, which include ZPVE and basis sets superposition error corrections, initially rise with the increasing number of water molecules, from 52 kJ mol^{-1} in the bare cation, $UO_2^+(O_2)$, to 67 kJ mol^{-1} in $UO_2^+(O_2)(H_2O)$, and to 80 kJ mol^{-1} in $UO_2^+(O_2)(H_2O)_2$ (Table 4). The presence of a third water molecule results in a slight decrease of the O_2 binding energy, to 74 kJ mol^{-1}. A similar trend was observed in a previous theoretical study,[35] in which the O_2 binding modes and energies were analyzed for $UO_2^+(O_2)(acetone)_n$ (n = 0−3). In that work, the strong η^2-O_2 binding to UO_2^+ and its successive solvates were described as two-electron three-atom

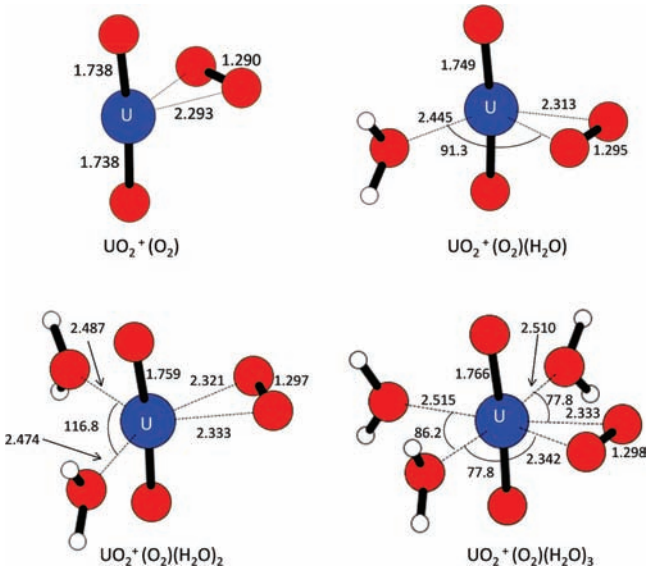

Figure 4. Lowest-energy optimized structures for $UO_2^+(O_2)(H_2O)_n$, n = 0−3. All of the species are in the doublet ground spin state.

Table 4. Computed Energy (ΔE^0) and Gibbs Free Energy (ΔG^{298}) Changes for the O_2 Addition Reactions[a]

reaction	UO_2^+	$UO_2^+\cdot(H_2O)$	$UO_2^+\cdot(H_2O)_2$	$UO_2^+\cdot(H_2O)_3$
ΔE^0	−52	−67	−80	−74
ΔG^{298}	−20	−24	−37	−26
reaction	NpO_2^+	$NpO_2^+\cdot(H_2O)$	$NpO_2^+\cdot(H_2O)_2$	$NpO_2^+\cdot(H_2O)_3$
ΔE^0	−24	−19	−16	−4
ΔG^{298}	2	12	15	28

[a]In kJ.mol^{-1}. The reactions correspond to the O_2 addition reactions: $AnO_2^+\cdot(H_2O)_n + O_2 \rightarrow AnO_2^+(O_2)(H_2O)_n$ for An = U, Np (n = 0−3). All reactants and products are in their ground state.

bonds, in which the increasing number of electron-donor acetone ligands strengthens the interaction energy with dioxygen; although water is a weaker Lewis base than acetone, a similar effect of increasing uranyl(V)−O_2 binding energy as donor ligands are added is to be expected and is observed.

The computed free energy of addition of inner-sphere O_2 to $UO_2^+\cdot(H_2O)_3$, −26 kJ mol^{-1}, a process which is observed, is slightly less favorable than that computed for the addition of an outer-sphere H_2O to $UO_2(OH)^+\cdot(H_2O)_3$, −29 kJ mol^{-1}, a process which is not observed. As remarked below, the results suggest that the DFT binding free energies of O_2 to UO_2^+ complexes may be significantly underestimated, by perhaps up to 30 kJ mol^{-1}. It should also be noted that the relative pressures of O_2 and H_2O in the ion trap are not known, though it is estimated that the pressures should be similar to within an order of magnitude.[3]

The lowest-energy $NpO_2^+(O_2)(H_2O)_n$ isomers are characterized by the presence of a dioxygen molecule in an η^1 mode (Figure 5). The O−O bond length is very close to that of the free O_2 molecule (1.206 Å at the B3LYP/SDD level of theory). Our calculations indicate that the open-shell singlet state (antiferromagnetic) computed using the broken-symmetry approach and the quintet spin state are practically degenerate in energy (within 4 kJ mol^{-1}), with the singlet state being slightly favored. The dioxygen binding energies are considerably lower than the corresponding values in the $UO_2^+(\eta^2\text{-}O_2)(H_2O)_n$ ions. The O_2 binding energy in $NpO_2^+(O_2)$ is ca.

dx.doi.org/10.1021/ic3001625 | Inorg. Chem. 2012, 51, 6603−6614

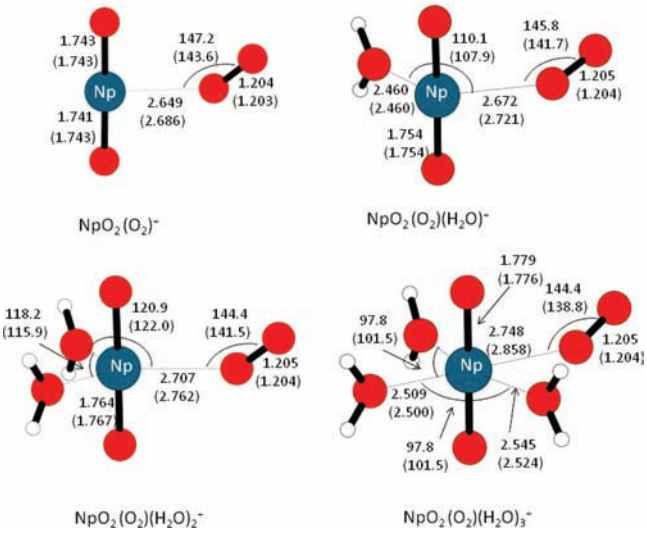

Figure 5. Lowest-energy optimized structures for $NpO_2^+(O_2)(H_2O)_n$, n = 0–3, in the (open-shell) singlet ground spin state and in the quintet spin state (in parentheses).

24 kJ mol^{-1}, and this binding energy decreases with the presence of water molecules, which is just the opposite trend observed for the $UO_2^+(\eta^2\text{-}O_2)(H_2O)_n$ superoxo complexes. The computed O_2 binding energies are 19 kJ mol^{-1} in $NpO_2^+(O_2)(H_2O)$, 16 kJ mol^{-1} in $NpO_2^+(O_2)(H_2O)_2$, and 4 kJ mol^{-1} in $NpO_2^+(O_2)(H_2O)_3$; the corresponding free energies for O_2 addition are all positive, from +2 kJ mol^{-1} for NpO_2^+ to +28 kJ mol^{-1} for $NpO_2^+\cdot(H_2O)_3$ (Table 4). A summary of NPA charges of all of the studied $AnO_2^+(O_2)(H_2O)_n$ ions is included as Supporting Information (Table S6).

In contrast to the uranyl–dioxygen superoxo complexes in which U^V has been oxidized to U^{VI}, the weakly bound neptunyl–dioxygen complexes evidently retain the Np^V oxidation state. The experimental observation of $UO_2^+(O_2)(H_2O)_n$ (n = 2 or 3) complexes but not $NpO_2^+(O_2)(H_2O)_n$ complexes is essentially a manifestation of the much lower VI/V reduction potential for U as compared with Np,[57] as discussed above. As the VI/V reduction potential for Pu (0.94 V) is substantially greater than that for U (0.09 V), but rather similar to that for Np (1.16 V), the nonobservation of $PuO_2^+(O_2)(H_2O)_n$ complexes can also be attributed to the relative inaccessibility of the Pu^{VI} oxidation state.

The addition of O_2 to $UO_2^+\cdot(H_2O)_n$ was only observed for n = 2 or 3, whereas the DFT results (Table 4) reveal that O_2 addition is also thermodynamically favorable for n = 0 or 1. A comparison of the free energies for the addition of H_2O and O_2 to $UO_2^+\cdot(H_2O)_n$ (Tables 2 and 4) reveals that H_2O addition is substantially more exoergic than O_2 addition for n = 0 or 1, in accord with the dominance of hydration. However, as H_2O addition to $UO_2^+\cdot(H_2O)_n$ remains substantially more exoergic (and exothermic) for n = 2 or 3, it is intriguing that O_2 addition is competitive with H_2O addition (see Figure 3) and is dominant for n = 3. As remarked below, this and other observations lead to the conclusion that the free energies for addition of O_2 to uranyl(V) hydrates are substantially more favorable than computed.

All of the reaction pathways analyzed for UO_2^+ complexes are summarized in Scheme 1. The species shown in Scheme 1 were isolated and reacted with O_2/H_2O as indicated. Among the species shown there, only $UO_2^+(O_2)(H_2O)$ and $UO_2^+\cdot(H_2O)_4$ could not be isolated, such that it is not known whether H_2O replaces O_2 in the first case, or vice versa in the latter case. However, the reversible reaction shown in the scheme was confirmed. Included in Scheme 1 are the reactions given by eqs 4, 5, and 6; the computed free energies at 298 K are reported here.

$$UO_2^+\cdot(H_2O)_2 + O_2 - X \rightarrow UO_2^+(O_2)(H_2O) + H_2O \quad \Delta G^{298} = +58 \text{ kJ mol} \tag{4}$$

$$UO_2^+(O_2)(H_2O)_3 + H_2O - X \rightarrow UO_2^+\cdot(H_2O)_4 + O_2 \quad \Delta G^{298} = -19 \text{ kJ mol} \tag{5}$$

$$UO_2^+(O_2)(H_2O)_2 + H_2O \leftrightarrow UO_2^+\cdot(H_2O)_3 + O_2 \quad \Delta G^{298} = -35 \text{ kJ mol} \tag{6}$$

The nonoccurrence of eq 4 is in accord with the computed free energy. Equation 5 is not observed but is computed to be exoergic, albeit by only −19 kJ mol; there may be a kinetic barrier to this exchange reaction for a monopositive uranyl ion with a coordination number of five: three monodentate H_2O ligands and one bidentate O_2. The forward reaction given by eq 6 is computed to be exoergic by −35 kJ mol and is observed; however, the reverse reaction is also observed, which suggests that this exchange reaction is close to thermoneutral (e.g., ΔG in the range of ca. ± 10 kJ mol^{-1}). The apparent discrepancy between computed energetic and experimental observations for eq 6 might reflect the greater uncertainties in DFT energies when a change in oxidation state is involved.[63−65] In particular, the DFT computations may somewhat underestimate, by ca. 30 kJ mol, the binding free energy of O_2 to $UO_2^+\cdot(H_2O)_2$. This possible error does not substantially affect the overall interpretations of the DFT results.

CONCLUSIONS

The monopositive actinyl ions $An^VO_2^+$ (An = U, Np, Pu) and $An^{VI}O_2(OH)^+$ (An = U, Pu) were produced by ESI; the gas-phase addition of water and dioxygen to these ions was studied by experimentation and DFT. The ESI yields of the actinyl(VI) ions, $UO_2(OH)^+ \gg PuO_2(OH)^+ > NpO_2(OH)^+$ (the last was not observed), directly reflect the stabilities of the An^{VI} relative to An^V: U ≫ Pu > Np. Gas-phase hydration of the actinyls

Scheme 1. Reactions of UO_2^+ Complexes with H_2O and O_2[a]

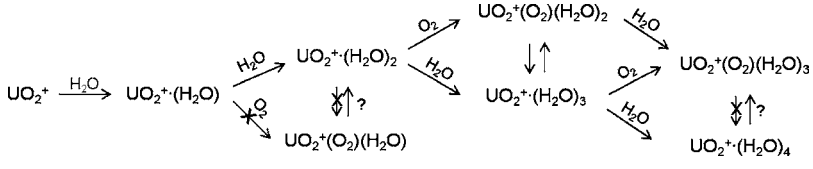

[a]Reactions marked with an "X" were not observed; reactions marked with a "?" could not be studied.

dx.doi.org/10.1021/ic3001625 | Inorg. Chem. 2012, 51, 6603–6614

terminated at $AnO_2^+\cdot(H_2O)_4$ and at $AnO_2(OH)^+\cdot(H_2O)_3$. DFT computations revealed that the next added water in both cases is outer-sphere for the lowest-energy structures; under our experimental conditions, only inner-sphere hydrates are observed. The inner-sphere actinyl hydration shell in the gas phase—i.e., the intrinsic elementary hydration—comprises one less water than in solution: $AnO_2^+\cdot(H_2O)_4\{gas\}$ versus $AnO_2^+\cdot(H_2O)_5\{aqueous\}$. This disparity is attributed to the "cooperative polarization effect" in solution,[9] whereby water is rendered a more effective electron-donor Lewis base due to electron donation from second-shell water molecules. The comparative hydration rates for the $AnO_2(OH)^+$ ions were more than one order of magnitude greater than for the AnO_2^+ ions, which is attributed to the additional vibrational degrees of freedom in the hydroxides for the dissipation of hydration energy to enable stabilization of the nascent hydrate by third-body collisional cooling. The $U^VO_2^+\cdot(H_2O)_n$ ions (n = 2 or 3) added O_2 to produce $UO_2^+(O_2)\cdot(H_2O)_n$; DFT revealed these to be superoxides in which uranium has been oxidized, formally $U^{VI}O_2^{2+}(\eta^2\text{-}O_2^-)(H_2O)_n$, with a substantial U-($\eta^2$-$O_2$) binding energy (i.e., >70 kJ mol^{-1}). Dioxygen addition was not observed for the corresponding neptunyl or plutonyl hydrates; DFT computations for the neptunyl species revealed that the most stable structures were $NpO_2^+(\eta^1\text{-}O_2)(H_2O)_n$, in which the Np-($\eta^1$-$O_2$) binding energy is small (i.e., <20 kJ mol^{-1}). The absence of superoxide formation for neptunyl(V) and plutonyl-(V) is a manifestation of the relatively large VI/V reduction potentials, 1.16 V for Np and 0.94 V for Pu, as compared with the value of 0.09 V for U.[57] The gas-phase results furthermore reveal condensed phase actinide chemistry,[66] including the contrasting prevalence of neptunyl(V)[67] and elusiveness of uranyl(V).[68] Among the aspects of gas-phase chemistry which will be pursued to elucidate and potentially advance condensed phase chemistry is the stabilization of neptunyl(VI) and plutonyl(VI) by the addition of O_2 to actinyl(V) coordination complexes with more strongly electron-donating ligands than water.

■ ASSOCIATED CONTENT

Supporting Information

Natural population analysis of the $AnO_2^+\cdot(H_2O)_n$ and $AnO_2(OH)^+\cdot(H_2O)_n^+$ ground-state ions. Complete thermodynamic information for the AnO_2^+ and $AnO_2(OH)^+$ hydration reactions. Measured actinyl hydration rates. Higher-energy isomers of the tetrahydrates of $AnO_2(OH)^+$ (An = U, Np, Pu) ions. Kinetics plot for the hydration of UO_2^+. Mass spectra demonstrating the addition of O_2 to UO_2^+ hydrates. ESI-QIT/MS experimental conditions used at ITN. Full citation for reference 49. Molecular coordinates of the $AnO_2^+\cdot(H_2O)_n$ and $AnO_2(OH)^+\cdot(H_2O)_n$ ground-state ions. This material is available free of charge via the Internet at http://pubs.acs.org.

■ AUTHOR INFORMATION

Corresponding Author

*E-mail: mc.michelini@unical.it; jkgibson@lbl.gov.

Notes

The authors declare no competing financial interest.

■ ACKNOWLEDGMENTS

Research was supported by the U.S. Department of Energy, Office of Basic Energy Sciences, Heavy Element Chemistry at LBNL, under Contract No. DE-AC02-05CH11231 [D.R., T.H.B., J.K.G.]; by the Università della Calabria [M.C.M]; and by the Fundação para a Ciência e a Tecnologia (acquisition of the QIT/MS at ITN and support as part of RNEM-Rede Nacional de Espectrometria de Massa, and Ph.D. grant SFRH/BD/70475/2010 to A.F.L.) [A.F.L., J.M.]. M.C.M. is grateful for the opportunity to be a Guest Scientist in the LBNL Chemical Sciences Division. The authors thank Dr. Guoxin Tian for providing the three actinyl stock solutions at LBNL. This research used resources of the National Energy Research Scientific Computing Center (NERSC), which is supported by the Office of Science of the U.S. Department of Energy under Contract No. DE-AC02-05CH11231.

■ REFERENCES

(1) Denning, R. G. *Struct. Bonding (Berlin)* **1992**, *79*, 215.
(2) Denning, R. G. *J. Phys. Chem. A* **2007**, *111*, 4125.
(3) Gresham, G. L.; Gianotto, A. K.; Harrington, P. D.; Cao, L. B.; Scott, J. R.; Olson, J. E.; Appelhans, A. D.; Van Stipdonk, M. J.; Groenewold, G. S. *J. Phys. Chem. A* **2003**, *107*, 8530.
(4) Chien, W.; Anbalagan, V.; Zandler, M.; Van Stipdonk, M.; Hanna, D.; Gresham, G.; Groenewold, G. *J. Am. Soc. Mass Spectrom.* **2004**, *15*, 777.
(5) Arnold, P. L.; Love, J. B.; Patel, D. *Coord. Chem. Rev.* **2009**, *253*, 1973.
(6) Antonio, M. R.; Soderholm, L.; Williams, C. W.; Blaudeau, J. P.; Bursten, B. E. *Radiochim. Acta* **2001**, *89*, 17.
(7) Skanthakumar, S.; Antonio, M. R.; Soderholm, L. *Inorg. Chem.* **2008**, *47*, 4591.
(8) Neuefeind, J.; Soderholm, L.; Skanthakumar, S. *J. Phys. Chem. A* **2004**, *108*, 2733.
(9) Bühl, M.; Sieffert, N.; Chaumont, A.; Wipff, G. *Inorg. Chem.* **2011**, *50*, 299.
(10) Spencer, S.; Gagliardi, L.; Handy, N. C.; Ioannou, A. G.; Skylaris, C. K.; Willetts, A.; Simper, A. M. *J. Phys. Chem. A* **1999**, *103*, 1831.
(11) Tsushima, S.; Suzuki, A. *THEOCHEM* **2000**, *529*, 21.
(12) Tsushima, S.; Suzuki, A. *Abstr. Annual Meeting of the Atomic Energy Society of Japan*; Atomic Energy Society of Japan: Japan, 1999; p 757.
(13) Hay, P. J.; Martin, R. L.; Schreckenbach, G. *J. Phys. Chem. A* **2000**, *104*, 6259.
(14) Tsushima, S.; Yang, T. X.; Suzuki, A. *Chem. Phys. Lett.* **2001**, *334*, 365.
(15) Vallet, V.; Wahlgren, U.; Schimmelpfennig, B.; Szabo, Z.; Grenthe, I. *J. Am. Chem. Soc.* **2001**, *123*, 11999.
(16) Clavaguera-Sarrio, C.; Hoyau, S.; Ismail, N.; Marsden, C. J. *J. Phys. Chem. A* **2003**, *107*, 4515.
(17) Clavaguera-Sarrio, C.; Brenner, V.; Hoyau, S.; Marsden, C. J.; Millie, P.; Dognon, J. P. *J. Phys. Chem. B* **2003**, *107*, 3051.
(18) Moskaleva, L. V.; Krüger, S.; Spörl, A.; Rösch, N. *Inorg. Chem.* **2004**, *43*, 4080.
(19) Cao, Z. J.; Balasubramanian, K. *J. Chem. Phys.* **2005**, *123*, 114309.
(20) Shamov, G. A.; Schreckenbach, G. *J. Phys. Chem. A* **2005**, *109*, 10961.
(21) Shamov, G. A.; Schreckenbach, G. *J. Phys. Chem. A* **2006**, *110*, 12072.
(22) Gutowski, K. E.; Dixon, D. A. *J. Phys. Chem. A* **2006**, *110*, 8840.
(23) Siboulet, B.; Marsden, C. J.; Vitorge, P. *Chem. Phys.* **2006**, *326*, 289.
(24) Vallet, V.; Macak, P.; Wahlgren, U.; Grenthe, I. *Theor. Chem. Acc.* **2006**, *115*, 145.
(25) Cao, Z. J.; Balasubramanian, K. *J. Chem. Phys.* **2009**, *131*, 164504.
(26) Tsierkezos, N. G.; Roithová, J.; Schröder, D.; Ončák, M.; Slavíček, P. *Inorg. Chem.* **2009**, *48*, 6287.
(27) Ončák, M.; Schröder, D.; Slavíček, P. *J. Comput. Chem.* **2010**, *31*, 2294.

(28) Schreckenbach, G.; Shamov, G. A. *Acc. Chem. Res.* **2010**, *43*, 19.
(29) Ramakrishnan, R.; Matveev, A. V.; Rösch, N. *Comput. Theor. Chem.* **2011**, *963*, 337.
(30) Allen, P. G.; Bucher, J. J.; Shuh, D. K.; Edelstein, N. M.; Reich, T. *Inorg. Chem.* **1997**, *36*, 4676.
(31) Alcock, N. W.; Esperas, S. *J. Chem. Soc., Dalton Trans.* **1977**, 893.
(32) Aberg, M.; Ferri, D.; Glaser, J.; Grenthe, I. *Inorg. Chem.* **1983**, *22*, 3986.
(33) Ramakrishnan, R.; Matveev, A. V.; Krüger, S.; Rösch, N. *Theor. Chem. Acc.* **2011**, *130*, 361.
(34) Groenewold, G. S.; Cossel, K. C.; Gresham, G. L.; Gianotto, A. K.; Appelhans, A. D.; Olson, J. E.; Van Stipdonk, M. J.; Chien, W. *J. Am. Chem. Soc.* **2006**, *128*, 3075.
(35) Bryantsev, V. S.; de Jong, W. A.; Cossel, K. C.; Diallo, M. S.; Goddard, W. A.; Groenewold, G. S.; Chien, W.; Van Stipdonk, M. J. *J. Phys. Chem. A* **2008**, *112*, 5777.
(36) Leavitt, C. M.; Bryantsev, V. S.; de Jong, W. A.; Diallo, M. S.; Goddard, W. A.; Groenewold, G. S.; Van Stipdonk, M. J. *J. Phys. Chem. A* **2009**, *113*, 2350.
(37) Bakac, A.; Espenson, J. H. *Inorg. Chem.* **1995**, *34*, 1730.
(38) Ricks, A. M.; Gagliardi, L.; Duncan, M. A. *J. Phys. Chem. Lett.* **2011**, *2*, 1662.
(39) Gronert, S. *J. Am. Soc. Mass Spectrom.* **1998**, *9*, 845.
(40) Rios, D.; Rutkowski, P. X.; Shuh, D. K.; Bray, T. H.; Gibson, J. K.; Van Stipdonk, M. J. *J. Mass Spectrom.* **2011**, *46*, 1247.
(41) Rutkowski, P. X.; Michelini, M. C.; Bray, T. H.; Russo, N.; Marçalo, J.; Gibson, J. K. *Theor. Chem. Acc.* **2011**, *129*, 575.
(42) Becke, A. D. *J. Chem. Phys.* **1993**, *98*, 5648.
(43) Lee, C. T.; Yang, W. T.; Parr, R. G. *Phys. Rev. B* **1988**, *37*, 785.
(44) Küchle, W.; Dolg, M.; Stoll, H.; Preuss, H. *J. Chem. Phys.* **1994**, *100*, 7535.
(45) de Jong, W. A.; Harrison, R. J.; Nichols, J. A.; Dixon, D. A. *Theor. Chem. Acc.* **2001**, *107*, 22.
(46) Krishnan, R.; Binkley, J. S.; Seeger, R.; Pople, J. A. *J. Chem. Phys.* **1980**, *72*, 650.
(47) Blaudeau, J. P.; McGrath, M. P.; Curtiss, L. A.; Radom, L. *J. Chem. Phys.* **1997**, *107*, 5016.
(48) Clark, T.; Chandrasekhar, J.; Spitznagel, G. W.; Schleyer, P. V. *J. Comput. Chem.* **1983**, *4*, 294.
(49) Frisch, M. J. et al. *Gaussian 09*; Gaussian Inc.: Wallingford, CT, 2009. See Supporting Information for full citation.
(50) Boys, S. F.; Bernardi, F. *Mol. Phys.* **1970**, *19*, 553.
(51) Norman, J. G.; Ryan, P. B.; Noodleman, L. *J. Am. Chem. Soc.* **1980**, *102*, 4279.
(52) Noodleman, L. *J. Chem. Phys.* **1981**, *74*, 5737.
(53) Ciofini, I.; Daul, C. A. *Coord. Chem. Rev.* **2003**, *238*, 187.
(54) Neese, F. *Coord. Chem. Rev.* **2009**, *253*, 526.
(55) Reed, A. E.; Curtiss, L. A.; Weinhold, F. *Chem. Rev.* **1988**, *88*, 899.
(56) Rutkowski, P. X.; Rios, D.; Gibson, J. K.; Van Stipdonk, M. J. *J. Am. Soc. Mass Spectrom.* **2011**, *22*, 2042.
(57) Konings, R. J. M.; Morss, L. R.; Fuger, J. In *The Chemistry of the Actinide and Transactinide Elements*, 3rd ed.; Morss, L. R., Edelstein, N. M., Fuger, J., Eds.; Springer: Dordrecht, The Netherlands, 2006; Vol. 4.
(58) Jones, L. H.; Penneman, R. A. *J. Chem. Phys.* **1953**, *21*, 542.
(59) Gibson, J. K.; Haire, R. G.; Santos, M.; Marçalo, J.; de Matos, A. P. *J. Phys. Chem. A* **2005**, *109*, 2768.
(60) Choppin, G. R.; Rao, L. F. *Radiochim. Acta* **1984**, *37*, 143.
(61) Cheng, P.; Koyanagi, G. K.; Böhme, D. K. *Chem. Phys. Chem.* **2006**, *7*, 1813.
(62) Cheng, P.; Koyanagi, G. K.; Böhme, D. K. *J. Phys. Chem. A* **2007**, *111*, 8561.
(63) Vallet, V.; Schimmelpfennig, B.; Maron, L.; Teichteil, C.; Leininger, T.; Gropen, O.; Grenthe, I.; Wahlgren, U. *Chem. Phys.* **1999**, *244*, 185.
(64) Di Santo, E.; Michelini, M. C.; Russo, N. *J. Phys. Chem. A* **2009**, *113*, 14699.
(65) Michelini, M. D.; Marçalo, J.; Russo, N.; Gibson, J. K. *Inorg. Chem.* **2010**, *49*, 3836.
(66) Edelstein, N. M.; Fuger, J.; Katz, J. J.; Morss, L. R. In *The Chemistry of the Actinide and Transactinide Elements*, 3rd ed.; Morss, L. R., Edelstein, N. M., Fuger, J., Eds.; Springer: Dordrecht, The Netherlands, 2006; Vol. 3.
(67) Copping, R.; Mougel, V.; Petit, S.; Den Auwer, C.; Moisy, P.; Mazzanti, M. *Chem. Commun.* **2011**, *47*, 5497.
(68) Graves, C. R.; Kiplinger, J. L. *Chem. Commun.* **2009**, 3831.
(69) Combes, J. M.; Chisholmbrause, C. J.; Brown, G. E.; Parks, G. A.; Conradson, S. D.; Eller, P. G.; Triay, I. R.; Hobart, D. E.; Meijer, A. *Environ. Sci. Technol.* **1992**, *26*, 376.